JOURNAL OF GEOPHYSICAL RESEARCH, VOL. 113, A11315, doi:10.1029/2008JA013539, 2008

Changes in the longitudinal structure of the low-latitude ionosphere during the July 2004 sequence of geomagnetic storms

N. M. Pedatella,[1] J. M. Forbes,[1] J. Lei,[1] J. P. Thayer,[1] and K. M. Larson[1]

Received 25 June 2008; revised 27 August 2008; accepted 29 September 2008; published 20 November 2008.

[1] In this brief report, the interplay between meteorological and geomagnetic activity influences on the low-latitude ionosphere is studied. Specifically, the disruption of the dominant wave-4 longitudinal structure of the equatorial ionization anomaly (EIA) by geomagnetic storms is investigated in connection with a sequence of three coronal mass ejections in July 2004. Observations of in situ electron density from the Challenging Minisatellite Payload (CHAMP) satellite are used to investigate changes in the longitudinal structure of the EIA during the different phases of the geomagnetic storms. The observed electron densities at ~1200 local time during the initial-main phases of the storms does not indicate significant longitudinal structure of the low-latitude ionosphere. A wave-4 structure of the EIA begins to reappear during the storm recovery phases although it is slightly weaker compared to undisturbed conditions. Although the upward propagating atmospheric tides responsible for generating the wave-4 structure of the EIA are not influenced by the geomagnetic storms, changes in the electric fields, neutral winds, and neutral composition due to the geomagnetic storms serve to disrupt the longitudinal structure of the EIA. The results further indicate that the sampling longitude needs to be accounted for when using satellite observations at a fixed local time for geomagnetic storm studies.

Citation: Pedatella, N. M., J. M. Forbes, J. Lei, J. P. Thayer, and K. M. Larson (2008), Changes in the longitudinal structure of the low-latitude ionosphere during the July 2004 sequence of geomagnetic storms, *J. Geophys. Res.*, *113*, A11315, doi:10.1029/2008JA013539.

1. Introduction

[2] The equatorial ionization anomaly (EIA) is a persistent feature of the low-latitude ionosphere, where the peaks in the electron density are found poleward of the geomagnetic equator. At low latitudes, neutral zonal winds in the thermosphere generate an eastward dynamo electric field during the daytime. The eastward electric field results in an upward $\mathbf{E} \times \mathbf{B}$ drift of the ionospheric plasma. Subsequent motion under the gravitational force results in the plasma traveling downward along the magnetic field lines and being deposited at locations north and south of the magnetic equator [*Appleton*, 1946]. Meridional neutral winds in the thermosphere drive plasma up and down field lines leading to a hemispheric asymmetry of the EIA during solstice time periods [*Schunk and Nagy*, 2000]. Any variability in the neutral winds, electric or magnetic fields therefore will directly impact the formation and strength of the EIA.

[3] Although previous observations showed that the low-latitude ionosphere exhibits longitudinal structure [*Chandra et al.*, 1973; *Mendillo et al.*, 2005; *Sagawa et al.*, 2005], *Immel et al.* [2006] were the first to connect the longitudinal structure to upward propagating tides. Both the F-region electron density and the latitudinal separation of the EIA peaks exhibit a wave-4 structure in longitude [*Immel et al.*, 2006]. The wave-4 structure begins to appear in electron density observations around 0800–1000 LT, is most evident in the late-afternoon hours, and disappears in the post-midnight hours [*Lin et al.*, 2007a, 2007b; *Scherliess et al.*, 2008]. A wave-4 structure can also be seen in the ionospheric peak height [*Lin et al.*, 2007b]. A seasonal dependence exists in the wave-4 structure and it is most apparent during equinox and June solstice, while it is not observed during December solstice [*Scherliess et al.*, 2008].

[4] The observed longitudinal variation in the EIA results from modulation of the thermospheric neutral winds due to nonmigrating tides of tropospheric origin. Longitudinal variations in the neutral winds subsequently generate a longitudinal variation in the E-region dynamo electric fields. Because the E-region electric fields can significantly impact the daytime F-layer, longitudinal variability in F-layer electron densities results [*Immel et al.*, 2006]. Results from the thermosphere-ionosphere-mesosphere-electrodynamics general circulation model (TIME-GCM) demonstrate that the wave-4 structure of the EIA can be explained by the effects of a diurnal eastward propagating tide with zonal wave number-3 (DE3) that is excited by

[1]Department of Aerospace Engineering Sciences, University of Colorado, Boulder, Colorado, USA.

0148-0227/08/2008JA013539$09.00

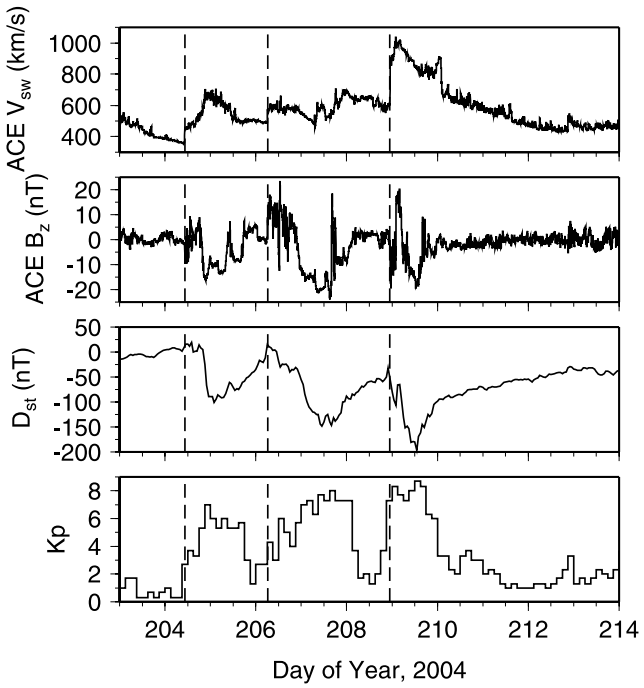

Figure 1. Solar wind and geophysical conditions during the sequence of geomagnetic storms in July 2004. Solar wind data are from the ACE spacecraft and are offset by 30 min. Dashed vertical lines indicate the time of sudden storm commencement.

latent heat release in the lower atmosphere [*Hagan et al.*, 2007]. When viewed at a fixed local time, DE3 appears as a wave-4 structure in longitude. In addition to DE3, the amplitude of other nonmigrating tides in the ionosphere dynamo region is significant during certain times of the year [*Forbes et al.*, 2008]. The effectiveness of these tides in modulating the dynamo electric fields in order to produce longitudinal structures in the F-region ionosphere has yet to be determined. However, as demonstrated by the modeling study of *England et al.* [2008], if these tides are capable of inducing a longitudinal structure in the dynamo electric fields a similar structure should exist in F-region electron densities.

[5] The upward propagating tides that are responsible for the longitudinal variability in the E-region dynamo electric fields are not influenced by changes in geomagnetic activity. However, the combination of prompt penetration [*Fejer*, 1997] and disturbance dynamo electric fields [*Blanc and Richmond*, 1980] along with changes in the neutral winds, composition and temperature [e.g., *Prölss 1980*; *Fuller-Rowell et al.*, 1994, 1996; *Lin et al.*, 2005; *Lei et al.*, 2008] significantly alter the low-latitude ionosphere during geomagnetic storms. It is therefore unclear how the wave-4 structure of the EIA is influenced by enhanced geomagnetic activity and how it changes with different phases of the storms. The objective of the present paper is to examine the evolution of the longitude structure of the low-latitude ionosphere during different phases of geomagnetic storms and also to discuss the interplay between different forcing mechanisms that may change the longitude structure. Changes in longitudinal structure are examined using in situ electron density measurements from the Planar Langmuir Probe (PLP) on board the Challenging Minisatellite Payload (CHAMP) satellite during a sequence of three geomagnetic storms that occurred during July 2004.

[6] The remainder of the paper is organized as follows. A brief overview of the solar wind and geophysical conditions during late July 2004 is given in section 2. Section 3 details the data sources as well as the method of analysis. In section 4, observations of in situ electron densities and an analysis of the how geomagnetic storms influence the longitudinal structure of the low-latitude ionosphere is presented. Conclusions are presented in section 5.

2. Solar Wind and Geophysical Conditions

[7] The time period of 19 July to 4 August 2004 (day of year 201–217) provides a serendipitous opportunity to observe the response of the equatorial ionosphere to relative changes in external forcing due to solar wind-magnetosphere-ionosphere coupling and coupling with thermal tides generated by latent heating due to deep tropical convection. During this period, DE3 modulation of the dynamo electric fields persisted [*Forbes et al.*, 2008] while changing solar wind conditions impact its influence on the low-latitude ionosphere. The changes in the solar wind conditions are described in detail below.

[8] Three geomagnetic storms occurred during the time period of 22–27 July 2004 due to a sequence of coronal mass ejections (CMEs) [*Zhang et al.*, 2007]. The solar wind and geophysical conditions associated with this time period are given in Figure 1. The solar wind data are from the ACE spacecraft and are offset by 30 min to account for the propagation of the solar wind from ACE to the magnetopause. All times referred to hereafter are the shifted time. The vertical dashed lines indicate the time of sudden storm commencement (SSC) (http://www.ngdc.noaa.gov/stp/SOLAR/ftpSSC.html). It is important to note that throughout this entire time period the $F10.7$ solar flux smoothly decayed from a high of 180.8 on 20 July to 87.9 on 4 August. Although this change is significant, it is not expected to impact the results as the longitudinal structure of the low-latitude ionosphere is fairly independent of solar flux conditions [*Scherliess et al.*, 2008].

[9] The first storm began at 1036 UT on 22 July 2004 as indicated by the first vertical dashed line in Figure 1. This is associated with an abrupt change in the solar wind velocity from ~370 km/s to ~460 km/s. The solar wind speed continued to increase for the next 12 h before beginning to decrease. The interplanetary magnetic field (IMF) B_z was northward for the first few hours which was followed by an extended period of southward B_z. The first storm reached a minimum D_{st} of −101 nT at 0300 UT on 23 July. The second storm began at 0613 UT on 24 July as identified by the change in the solar wind velocity from ~490 km/s to ~570 km/s. Following the shock in the solar wind, the IMF B_z was northward for nearly 11 h before turning to the south. A minimum D_{st} of −148 nT was reached at 1200 UT on 25 July. A significant change in the solar wind velocity from ~600 km/s to ~900 km/s at 2249 UT on 26 July marked the beginning of the third storm. The IMF B_z was initially southward for the first few hours. This was followed by a short period of northward B_z before an extended

period of southward B_z. At 1400 UT on 27 July, a minimum D_{st} of −197 nT was reached. Owing to these differences, the overall ionospheric response is expected to be different for each storm. However, this sequence of storms provides the opportunity to investigate changes in longitudinal structure of the low-latitude ionosphere without needing to account for changes that are due to seasonal or local time effects.

[10] Geomagnetic storms can typically be divided into an initial, main, and recovery phase. The initial phases for the three storms are from 1036 UT on 22 July to 19 UT on 22 July, from 0613 UT on 24 July to 2130 UT on 24 July, and from 2249 on 26 July to 0500 UT on 27 July. The main phase follows the initial phase and is considered to end when the minimum D_{st} is reached. For the first two storms, the recovery phase is considered to extend from the time of minimum D_{st} to 1 h prior to the beginning of the following storm. The recovery phase of the third storm is considered to last until 31 July.

3. Data and Analysis

[11] The CHAMP satellite was launched on 15 July 2000 into a nearly circular orbit with an inclination of 87.5 degrees and an initial altitude of 450 km. The primary mission of CHAMP is to study the gravity and magnetic fields of the Earth. A variety of instrumentation is on board the CHAMP satellite, including an accelerometer, a GPS radio occultation receiver, magnetometers, and a PLP [*Reigber et al.*, 2002]. CHAMP is in a nearly Sun-synchronous orbit and it precesses in local time at the rate of ∼5.44 min per day. The near Sun-synchronous orbit of the CHAMP satellite allows it to sample the same local time at 15–16 different longitudes during one day, making it suitable for observing the wave-4 structure of the EIA. During late July 2004, CHAMP observed local times of roughly noon and midnight and was at an altitude of ∼380 km. The longitudinal structure of the EIA during quiet times is more apparent in the in situ electron density measurements at local noon than at local midnight and we have, therefore, focused only on the measurements at local noon.

[12] In situ electron density data can be derived from the PLP on board the CHAMP satellite [*Rother et al.*, 2004]. Processed electron density data from the PLP are available from the Information Systems and Data Center operated by GeoForschungsZentrum (GFZ) Potsdam (http://isdc.gfz-potsdam.de). Electron density measurements are taken every 15 s, which corresponds to an in-track distance of ∼120 km. It is important to recognize the fact that the electron densities are at the location of the CHAMP satellite. This is a limitation of the data set in that the same region of the ionosphere is not always being sampled owing to changes in the F-layer peak height and variations in the CHAMP orbital altitude, which can be as large as 10–15 km over one orbit. The effect of changes in the orbital altitude in the region of ±30° latitude on the observed electron densities are thought to be insignificant compared to the potentially large changes in the F-layer peak height that occur during geomagnetic storms. Despite these limitations it is believed that the in situ electron density measurements provide a useful data set for observing changes in the longitudinal structure of the EIA due to geomagnetic disturbances.

[13] For the present study, we calculate the crest-to-trough ratio (CTR) (equation (1)) for each dayside CHAMP orbit to indicate the strength of the EIA [*Lühr et al.*, 2007; *Mendillo et al.*, 2000].

$$CTR = \frac{n_{e,n} + n_{e,s}}{2n_{e,t}} \tag{1}$$

where, $n_{e,n}$ and $n_{e,s}$ are the electron densities of the north and south peaks and $n_{e,t}$ is the electron density of the equatorial trough. The electron density profile for each orbit can then be associated with the CTR and the equatorial crossing longitude. Note that the CTR is set to 1 when the EIA has not been well established.

4. Results and Discussion

4.1. CHAMP Observations of in Situ Electron Densities

[14] Figure 2 shows the in situ electron densities at ∼1200 LT during the storm time period. The observations on day 203 show peaks in the EIA strength near longitudes of 0, 90, 180 and 270 degrees, demonstrating that the wave-4 structure is observed during the geomagnetically quiet period prior to the first storm. A slight hemispheric asymmetry can be seen, presumably due to the thermospheric circulation from the summer hemisphere to the winter hemisphere. It is also evident that the strength of the EIA is greatest over the Asian sector (∼90 degrees) which has previously been observed during summer solstice [*Scherliess et al.*, 2008].

[15] The response to the geomagnetic storms can be seen on days 204–210 in Figure 2. Significant changes in the longitudinal structure of the EIA occur during this time period. On days 204, 207, and 209, the longitudinal structure is no longer evident during the initial and main phases of the storms when K_p is increasing and D_{st} is decreasing. Looking at the end of day 205, the beginning of day 206, and day 208 it is apparent that a longitudinal structure begins to reappear rather quickly following the main phase of the storms. Beginning on day 211 the reemergence of the wave-4 structure of the EIA is clearly observed as the ionosphere returns to an undisturbed state.

[16] To illustrate the prominence of the wave-4 structure, a Fourier fit in longitude is performed using the dayside CTR values to determine the amplitudes and phases for wave numbers 1–7. We will first look at the longitude structure during the geomagnetically quiet time periods consisting of days 200–203 and 213–217. Average dayside CTR values are obtained by placing the data into 10 degree longitude bins. A Fourier fit is then performed using the average CTR values and the resulting amplitudes are shown in Figure 3. As expected, the primary component of the CTR is wave number-4 during undisturbed time periods. Wave number-1 is the second strongest component which is likely due to the enhancement of the EIA that occurs over the Asian sector during summer solstice.

[17] Now we turn to the investigation of how the longitudinal structure changes with geomagnetic activity. During quiet times, a Fourier fit in longitude is performed using the

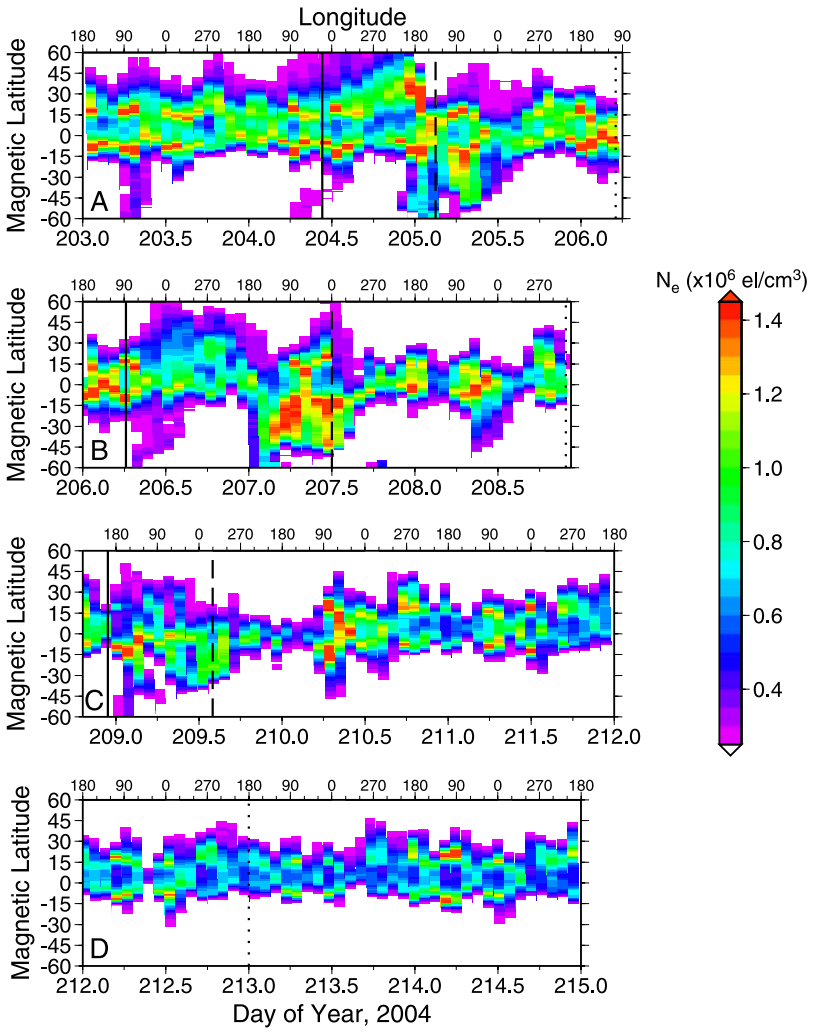

Figure 2. In situ electron density measurements from the PLP on board the CHAMP satellite at ~1200 LT. Solid, dashed, and dotted vertical lines indicate the times of sudden storm commencement, minimum D_{st}, and the end of the recovery phase, respectively. White areas indicate electron densities less than 0.3×10^6 el/cm^3.

dayside CTR values from a single day to determine the amplitudes and phases of wave numbers 1–5. During the disturbed time period, we compute a separate wave number spectrum using the CTR values during the recovery phase of each storm as well as the initial-main phase of the second storm. This is done because of the rapid changes that occur during each phase of a geomagnetic storm. Owing to insufficient longitude coverage a wave number spectrum cannot be computed during the initial-main phases of the first and third storm. In the event that an orbit overlaps storm periods, we neglect this pass entirely. Figure 4 shows the resulting wave number spectrum, where each spectrum has been normalized to a maximum value of one in order to show the relative importance of each wave number.

[18] It can again be seen in Figure 4 that the primary component of the CTR is wave number-4 during the quiet time period before and after the sequence of storms. A significant wave number-2 component is also present on certain days. Day-to-day variability in the relative amplitude of the wave number-4 component is evident during the undisturbed time period, however it should be noted that the dominant structure is always wave-4 during the quiet time periods. In addition to variability in the equatorial electric field strength, the daily variability may partly be due to the fact that the wave number spectrum for a given day is computed using a limited number of CTR values owing to the longitudinal sampling of the CHAMP satellite.

[19] As shown in Figure 4, during the initial and main phases of the second storm, the wave number spectrum is dominated by wave number-2 instead of wave number-4. It is also apparent in Figure 2 that a significant longitudinal structure is not present during the initial-main phases of the first and third storms. Figure 4 shows that wave number-4 reemerges as the primary component during the recovery phase of each storm. Potential causes for the disruption and reappearance of the longitudinal structure of the EIA are discussed in detail in the following section.

4.2. Discussion

[20] The in situ electron densities previously presented clearly demonstrate that the wave-4 structure observed during quiet times is disrupted by the geomagnetic storms.

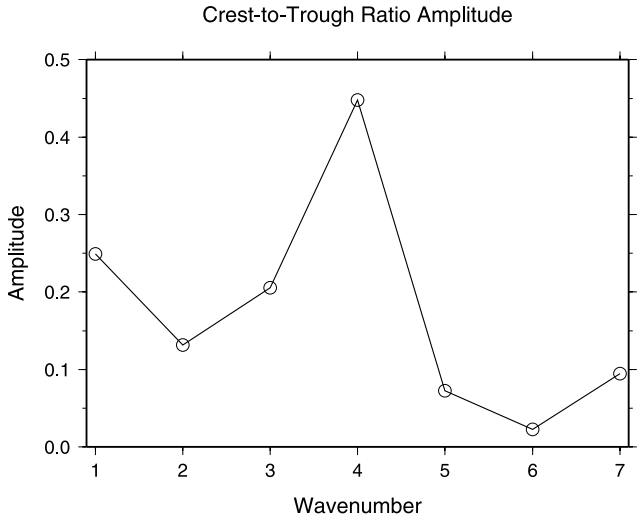

Figure 3. Wave number spectrum of the crest-to-trough ratio during the geomagnetically quiet time periods before and after the sequence of geomagnetic storms. In situ electron density measurements from days 200–203 and 213–217 are averaged prior to computing the wave number spectrum.

This is evident in Figure 4, where the only time periods when wave-4 does not dominate is during the initial-main phase of the second storm. The potential causes for the modulation of the wave-4 structure are now discussed in greater detail. The main forcing mechanism for the observed wave-4 structure is the DE3 tide that is excited by latent heat release in the low-latitude troposphere [*Hagan et al.*, 2007]. Upward propagating tides influence the E-region dynamo electric fields generating the longitudinal variation in the EIA. As the geomagnetic storms may not affect generation of the DE3 tide, the forcing mechanism for the wave-4 structure remains present throughout the disturbed time period. The disruption of the wave-4 structure can therefore be attributed to changes in the electric fields, thermospheric winds and neutral composition associated with geomagnetic activity.

[21] Penetration and dynamo electric fields are two potential mechanisms responsible for disrupting the wave-4 structure of the EIA. The penetration of the magnetospheric electric fields has significant effects on ionospheric electrodynamics at low and middle latitudes [*Kelley*, 1989]. During the initial phase of geomagnetic storms, the prompt penetration electric fields cause an increased upward drift and an expansion of the EIA at noon local times [*Mendillo*, 2006]. By comparing the Coupled Magnetosphere Ionosphere Thermosphere model simulations with those from GPS TEC observations, *Lei et al.* [2008] showed that penetration electric fields were the primary process that produced the observed TEC enhancements during the initial phase of the December 2006 storm event. The significantly enhanced electron density and expanse of the EIA crests around 2000 UT on day 204, 0800 UT on day 206, and 0000 UT on day 209 in Figure 2 may be related to penetration electric fields during the beginning stages of these storms. The greater eastward electric field strength will also result in the observed enhancement of the EIA at all longitudes. If the strength of the prompt penetration electric fields is greater than the quiet time fields, they dominate the EIA formation and are able to eliminate the quiet time longitudinal structure of the EIA. It is interesting to note that disturbance dynamo electric fields might not play a major role in the changes of the wave structure during the storm periods, which will be discussed later.

[22] In addition to changes in the electric fields, changes in the neutral winds and composition are likely to disrupt the longitudinal structure of the EIA, especially during the storm main phase. Around local noon, storm time neutral winds have been observed to be predominantly equatorward [*Emmert et al.*, 2004]. The strong equatorward winds move the plasma along the magnetic field lines to higher altitude where the recombination rate is lower and then increase electron density. This will result in an increase in the observed electron densities at the nearly fixed altitude of the CHAMP satellite. On the other hand, they also can prevent the ionospheric plasma from diffusing down field lines resulting in electron density enhancements in the EIA [e.g., *Lei et al.*, 2007; *Lin et al.*, 2005]. Furthermore, the response of the F2 peak electron densities and neutral composition change considerably with season [e.g., *Prölss*, 1980; *Fuller-Rowell et al.*, 1996]. Negative storm effects in electron density extend to much lower latitudes in the summer hemisphere than they do in the winter hemisphere, whereas positive storm effects are much more likely to be seen in the winter hemisphere, particularly in the middle of the day. Signatures of this can be seen in Figure 2 during the main phase of the first storm around 0500–1000 UT on day 205. This is also evident during the main phase of the second storm during the time period 0400–1300 UT on day

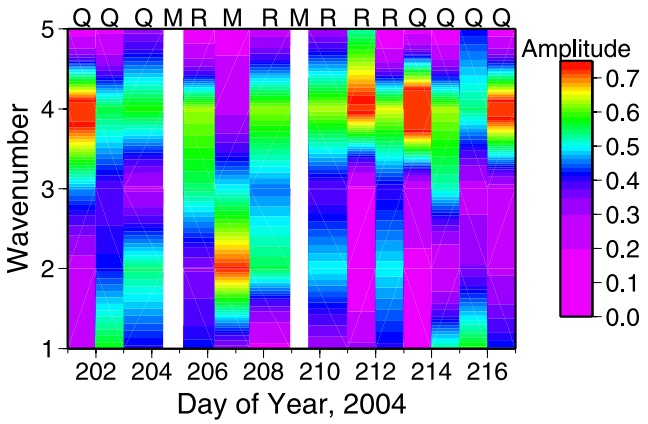

Figure 4. Wave number spectra of the crest-to-trough ratio. The letters Q (quiet), M (initial-main), and R (recovery) along the top indicate the phase of the storm. During the geomagnetically quiet time periods one wave number spectra is computed for each day. During the geomagnetic storms, separate wave number spectra are computed for the initial-main phase of the second storm and for the recovery phases of each storm. The white bands are due to insufficient longitudinal coverage making it impossible to compute a wave number spectra during the initial-main phases of the first and third storm. Each spectra is normalized in order to show the relative importance of each wave number.

207. During these time periods a significant electron density enhancement is observed the southern hemisphere. This hemispheric asymmetry of the electron density enhancement can be attributed to the storm time equatorward winds as well as changes in the neutral composition.

[23] During the storm recovery phase, the primary driver for the variations of the low-latitude ionosphere will likely no longer be the eastward prompt penetration electric fields, but rather the disturbed neutral winds and the resultant westward disturbance dynamo electric fields [*Blanc and Richmond*, 1980]. At noon local time this results in a downward $\mathbf{E} \times \mathbf{B}$ drift and a contraction of the EIA [*Mendillo*, 2006]. Therefore, it is surprising that during the recovery phase of each storm wave number-4 reemerges as the primary component. This may indicate that slowly changing disturbance neutral winds and the corresponding dynamo electric fields allow the upward propagating tides to influence the electric fields resulting in the reemergence of wave number-4 as the primary component during the recovery phase. The westward disturbance dynamo electric fields also suppress the strength of the EIA. The suppression of the EIA strength can be observed in Figure 2 during the recovery phase of each storm. This is particularly evident beginning around 1500 UT on day 209 during the recovery phase of the third storm.

[24] Although the mechanisms thought to be responsible for the disruption of the wave-4 structure of the EIA during the initial and main phases of geomagnetic storms have been discussed, the relative importance of each is still unknown. Moreover, we can only postulate that DE3 is capable of modulating the disturbance neutral winds and disturbance dynamo electric fields, leading to the reemergence of the wave-4 structure during the recovery phase of the storms. A more detailed study involving additional data sources and modeling is therefore necessary. It is also unclear if similar changes in the longitudinal structure of the EIA due to geomagnetic storms would occur during different seasons and local times.

5. Conclusions

[25] The results presented here demonstrate the disruption of the wave-4 structure of the EIA that arises owing to geomagnetic storms. Although the forcing mechanism responsible for generating the wave-4 structure remains present during the disturbed time period, the dramatic changes in electric fields, neutral winds and composition eliminate the observed longitudinal structure during the initial-main phases of the storms. During the storm recovery phase the wave-4 structure reemerges in the EIA. Further investigations are required to understand the mechanisms which are responsible for the different longitude structure of the EIA during different phases of the storms. Modeling studies may be able to determine the primary cause of the disruption of the longitudinal structure of the EIA during the initial-main phases. Additional modeling could also answer the question of whether or not DE3 is able to modulate the disturbance neutral winds and disturbance dynamo electric fields. Multi-diagnostic measurements of electric fields, plasma densities, and neutral winds and composition are also necessary in order to further our understanding of how the longitudinal structure of the low-latitude ionosphere is impacted by geomagnetic storms.

[26] The results have implications for future storms studies that use satellite measurements at a fixed local time. When looking at the initial response due to geomagnetic storms using these data sets it is important to compare the storm time observations with quiet time observations at the same longitude. If observations from sequential orbits are used the observed enhancements may be biased owing to the sampling longitude of the satellite. For example, if on the orbit immediately prior to a storm CHAMP is at a longitude of enhanced EIA strength, the observed change in the electron densities due to the storm may be less than if prior to the storm CHAMP was at a longitude of decreased EIA strength. Not accounting for this may result in an inaccurate determination of the ionospheric response to a geomagnetic storm. This problem can be avoided if observations taken at the same longitude and local time are compared.

[27] **Acknowledgments.** This work was supported in part by grant ATM-0719480 from the National Science Foundation as part of the Space Weather Program and by grant EAR-0538116. The authors thank the providers of data used for the present study: GFZ-Potsdam for making available in situ electron density measurements and the NGDC for ACE solar wind and geophysical data.

[28] Zuyin Pu thanks the reviewers for their assistance in evaluating this paper.

References

Appleton, E. V. (1946), Two anomalies in the ionosphere, *Nature*, *157*, 691.

Blanc, M., and A. D. Richmond (1980), The ionospheric disturbance dynamo, *J. Geophys. Res.*, *85*, 1669–1680.

Chandra, S., E. I. Reed, B. E. Troy Jr., and J. E. Blamont (1973), Equatorial airglow and the ionospheric geomagnetic anomaly, *J. Geophys. Res.*, *78*(22), 4630–4640.

Emmert, J. T., B. G. Fejer, G. G. Sheperd, and B. H. Solheim (2004), Average nighttime F region disturbance neutral winds measured by UARS WINDII: Initial results, *Geophys. Res. Lett.*, *31*, L22807, doi:10.1029/2004GL021611.

England, S. L., T. J. Immel, and J. D. Huba (2008), Modeling the longitudinal variation in the post-sunset far-ultraviolet OI airglow using the SAMI2 model, *J. Geophys. Res.*, *113*, A01309, doi:10.1029/2007JA012536.

Fejer, B. G. (1997), The electrodynamics of the low-latitude ionosphere: recent results and future challenges, *J. Atmos. Sol. Terr. Phys.*, *59*(13), 1465–1482.

Forbes, J. M., X. Zhang, S. Palo, J. Russell, C. J. Mertens, and M. Mlynczak (2008), Tidal variability in the ionospheric dynamo region, *J. Geophys. Res.*, *113*, A02310, doi:10.1029/2007JA012737.

Fuller-Rowell, T. J., M. V. Codrescu, R. J. Moffett, and S. Quegan (1994), Response of the thermosphere and ionosphere to geomagnetic storms, *J. Geophys. Res.*, *99*, 3893–3914.

Fuller-Rowell, T. J., M. V. Codrescu, H. Rishbeth, R. J. Moffett, and S. Quegan (1996), On the seasonal response of the thermosphere and ionosphere to geomagnetic storms, *J. Geophys. Res.*, *101*(A2), 2343–2353.

Hagan, M. E., A. Maute, R. G. Roble, A. D. Richmond, T. J. Immel, and S. L. England (2007), Connections between deep tropical clouds and the Earth's ionosphere, *Geophys. Res. Lett.*, *34*, L20109, doi:10.1029/2007GL030142.

Immel, T. J., E. Sagawa, S. L. England, S. B. Henderson, M. E. Hagan, S. B. Mende, H. U. Frey, C. M. Swenson, and L. J. Paxton (2006), Control of equatorial ionospheric morphology by atmospheric tides, *Geophys. Res. Lett.*, *33*, L15108, doi:10.1029/2006GL026161.

Kelley, M. C. (1989), *The Earth's Ionosphere: Plasma Physics and Electrodynamics*, Academic, San Diego, Calif.

Lei, J., et al. (2007), Comparison of COSMIC ionospheric measurements with ground-based observations and model predictions: Preliminary results, *J. Geophys. Res.*, *112*, A07308, doi:10.1029/2006JA012240.

Lei, J., W. Wang, A. G. Burns, S. C. Solomon, A. D. Richmond, M. Wilberger, L. P. Goncharenko, A. Coster, and B. W. Reinisch (2008), Observations and simulations of the ionospheric and thermo-

spheric response to the December 2006 geomagnetic storm: Initial phase, *J. Geophys. Res.*, *113*, A01314, doi:10.1029/2007JA012807.

Lin, C. H., A. D. Richmond, R. A. Heelis, G. J. Bailey, G. Lu, J. Y. Liu, H. C. Yeh, and S. Y. Su (2005), Theoretical study of the low- and mid-latitude ionospheric electron density enhancement during the October 2003 superstorm: Relative importance of the neutral wind and the electric field, *J. Geophys. Res.*, *110*, A12312, doi:10.1029/2005JA011304.

Lin, C. H., W. Wang, M. E. Hagan, C. C. Hsiao, T. J. Immel, M. L. Hsu, J. Y. Liu, L. J. Paxton, T. W. Fang, and C. H. Liu (2007a), Plausible effect of atmospheric tides on the equatorial ionosphere observed by the FORMOSAT-3/COSMIC: Three-dimensional electron density structures, *Geophys. Res. Lett.*, *34*, L11112, doi:10.1029/2007GL029265.

Lin, C. H., C. C. Hsiao, J. Y. Liu, and C. H. Liu (2007b), Longitudinal structure of the equatorial ionosphere: Time evolution of the four-peaked EIA structure, *J. Geophys. Res.*, *112*, A12305, doi:10.1029/2007JA012455.

Lühr, H., K. Hausler, and C. Stolle (2007), Longitudinal variation of *F* region electron density and thermospheric zonal wind caused by atmospheric tides, *Geophys. Res. Lett.*, *34*, L16102, doi:10.1029/2007GL030639.

Mendillo, M. (2006), Storms in the ionosphere: Patterns and processes for total electron content, *Rev. Geophys.*, *44*, RG4001, doi:10.1029/2005RG000193.

Mendillo, M., L. Bosheng, and J. Aarons (2000), The application of GPS observations to equatorial aeronomy, *Radio Sci.*, *35*(3), 885–904.

Mendillo, M., C. Huang, X. Pi, H. Rishbeth, and R. Meier (2005), The global ionospheric asymmetry in total electron content, *J. Atmos. Sol. Terr. Phys.*, *67*(15), 1377–1387, doi:10.1016/j.jastp.2005.06.021.

Prölss, G. W. (1980), Magnetic storm associated perturbations of the upper atmosphere—Recent results obtained by satellite-born gas analyzers, *Rev. Geophys. Space Phys.*, *18*, 183–202.

Reigber, C., H. Luhr, and P. Schwintzer (2002), CHAMP mission status, *Adv. Space Res.*, *30*(2), 129–134.

Rother, M., S. Choi, W. Mai, H. Luhr, and D. Cooke (2004), Status of the CHAMP ME data processing, in *Earth Observation With CHAMP: Results From Three Years in Orbit*, edited by C. Reigber et al., pp. 413–418, Springer, New York.

Sagawa, E., T. J. Immel, H. U. Frey, and S. B. Mende (2005), Longitudinal structure of the equatorial anomaly in the nighttime ionosphere observed by IMAGE/FUV, *J. Geophys. Res.*, *100*, A11302, doi:10.1029/2004JA010848.

Scherliess, L., D. C. Thompson, and R. W. Schunk (2008), Longitudinal variability of low-latitude total electron content: Tidal influences, *J. Geophys. Res.*, *113*, A01311, doi:10.1029/2007JA012480.

Schunk, R. W., and A. F. Nagy (2000), *Ionospheres: Physics, Plasma Physics, and Chemistry*, Cambridge Univ. Press, New York.

Zhang, J., et al. (2007), Solar and interplanetary sources of major geomagnetic storms ($D_{st} \leq -100$ nT) during 1996–2005, *J. Geophys. Res.*, *112*, A10102, doi:10.1029/2007JA012321.

J. M. Forbes, K. M. Larson, J. Lei, N. M. Pedatella, and J. P. Thayer, Department of Aerospace Engineering Sciences, University of Colorado, 429 UCB, Boulder, CO 80309, USA. (nicholas.pedatella@colorado.edu)